Next Materials 1 (2023) 100028

Contents lists available at ScienceDirect

Next Materials

journal homepage: www.sciencedirect.com/journal/next-materials

Research article

Low temperature sulfonated biochar from Macauba's endocarp for lead adsorption from wastewater

Izabela Sabrina Souza De Brito[a], Clésia Cristina Nascentes[a], Paula Sevenini Pinto[b], Fabiano Gomes Ferreira de Paula[a], Ana Paula de Carvalho Teixeira[a,*]

[a] Universidade Federal de Minas Gerais (UFMG), Av. Antônio Carlos, 6627, Belo Horizonte 31270-901, Minas Gerais, Brazil
[b] Universidade do Estado de Minas Gerais (UEMG), Av. Paraná, 3001, Divinópolis 35501-170, Minas Gerais, Brazil

ARTICLE INFO

Keywords:
Sulfonated biochar
Adsorption
Macauba endocarp
Lead removal

ABSTRACT

Lead is a heavy metal that can be present in different types of effluents. This toxic ion is harmful both to human health and to other species. Therefore, it is necessary to study materials that can be used to remove lead from aquatic environments. In this context, the use of modified biomass residues for the production of efficient adsorbents for this purpose stands out. In this work was synthesized a new type of adsorbent material, sulfonated carbon, from macauba oil extraction residue for application in the removal of lead ions from aqueous media. The sulfonated carbons were produced from the reaction of macauba endocarp with concentrated sulfuric acid at 100 °C at 1, 2 and 4 h. The materials were characterized by XRD, MS-TG, Raman and infrared spectroscopies, SEM, potential titration, elemental analysis and by N_2 adsorption/desorption. All synthetic conditions were efficient to produce functionalized carbonaceous materials with amorphous characteristics and good thermal stability. Although the material carbonized for 4 h had a low specific surface area (2 $m^2.g^{-1}$), it showed the higher efficiency for the removal of lead ions from aqueous solution. The adsorption occurred due to interactions of these ions with the functional groups present on the surface of the coal. The greatest lead removal occurred at pH 5.0 (83.8%), where –COOH and SO_3H groups are in the deprotonated form, what favors the electrostatic attraction of Pb^{2+} ions. The experimental results were fitted using pseudo-first-order and pseudo-second-order models. A high concentration of lead ions was removed in the first 40 min, and the removal percentage was 97.5% for the less concentrated solution (10 mg·L^{-1}) and 55.0% for the solution with the highest concentration (100 mg·L^{-1}). The increase in the concentration of adsorbent provided an increase in the removal of this contaminant. The isotherm of adsorption was adjusted by Langmuir and Freundlich models. The better adjust was obtained by Langmuir and the maximum adsorption capacity by this model was 104.2 mg·g^{-1}. The best lead removal conditions were: adsorbent concentration: 0.5 g.L^{-1}; pH 5; Pb^{2+} concentration 80 mg.L^{-1} and time 2 h.

Introduction

The presence of heavy metals in wastewater is a major concern due to its nonbiodegradability and toxicity to the environment and human beings [1,2]. The toxic metals of great interest in wastewater treatment are lead, copper, cadmium, chromium, zinc, and nickel [2,3].

Lead is used in different industry segments such as painting, pesticides, batteries, mining, shooting ranges, plumbing installations, or repair sites [4,5]. For humans, lead can cause severe damage to the kidneys, nervous system, liver, and brain [6,7]. It is then necessary to develop efficient strategies to remove it from the environment [8].

Several methods are described such as chemical precipitation [9], electrochemical, [10] flotation, [11] filtration, [12] and adsorption [13]. Among these, adsorption is one of the most promising due to its simplicity and low cost [14].

In this context, it is worth highlighting the works in the literature on different functionalized materials, based on mesoporous silicas, for the removal of lead ions. These materials have been used for the production of sensors and other systems for the adsorption of this toxic metal with results that stand out compared to other compounds [15–25].

In addition to materials based on functionalized inorganic materials, there is in the literature the use of biomass for the production of adsorbents for heavy metals [26]. This use is an interesting alternative for generating materials with higher added value from biomass residues,

* Corresponding author.
E-mail address: anapct@ufmg.br (A.P.d.C. Teixeira).

https://doi.org/10.1016/j.nxmate.2023.100028
Received 22 March 2023; Received in revised form 12 June 2023; Accepted 23 June 2023

that is an important environmental problem nowadays. In this context, biochar is a promising alternative for Pb and other heavy metals adsorption from wastewater [26].

However, its synthesis usually depends on high temperatures (400–800 °C) under inert temperatures followed by chemical or physical activation. Such high-demand energy processes increase the overall cost of these materials [13,27].

Few works in literature have been describing the production of biochar by low-temperature processes and air atmosphere [28,29]. Yu et al. prepared sulfonated biochar from the fast-growing herb *Axonopus compressus* for Pb(II) and Cd(II) removal from wastewater [28]. After crushed and dried, the herb particles were mixed with H_2SO_4 at 180 °C in air atmosphere for 30 min. Zhao et al. used pomelo peel as a carbon source for sulfonated biochar. The dry pomelo peel powder was impregnated with H_2SO_4 and carbonized for 2 h at 250 °C and the obtained material was used for Ag(I) and Pb(II) adsorption. [29].

These materials, in addition to being produced in low temperature and air atmosphere, were also functionalized. Such modifications have attracted attention due to its potential of high adsorption levels, because of interactions between the analyte and the functional groups in the carbon surface [30–32]. Yang et al. obtained biochar with amino groups in its surface for Cu ions adsorption in water solution [33]. They showed an increase (5–8-folds) in adsorption capacity after strong complexation between Cu and amino groups.

Another important consideration concerning biochar adsorbents is the carbon source [34]. Usually, agricultural wastes are the preferred choice because of their high availability and low cost [28,29,35]. In Brazil, macauba (Acrocomia aculeata) is considered an oilseed with a high potential for biodiesel production because of its high oil content [36,37]. However, a drawback is the amount of residual biomass after oil extraction [38].

In this work, a low-temperature and air atmosphere process was used for the production of sulfonated biochar (SB) from the residual biomass macauba's endocarp. The obtained SB was then used for Pb(II) adsorption from aqueous solution. The effect of adsorbent initial concentration and pH were evaluated, as well isotherm and kinetics experiments were studied in order to understand the adsorption mechanism.

Materials & methods

Synthesis of biochar

Powdered (100–200 mesh) macauba's endocarp (MEP) was gently donated by Paradigma Óleos Vegetais. The material was used without further treatment.

For biochar production, MEP was first added to concentrated H_2SO_4 (98% Anidrol) in 1 g:16 mL ratio. The mixture was then stirred at 100 °C in an oil bath using different times, 1, 2, and 4 h. The material was filtered and washed with distilled water until pH 7. Then, it was dried at 60 °C for 24 h, milled and labelled BC01, BC02 and BC04, based on the time in contact with acid (1, 2 or 4 h, respectively).

Characterization

The produced biochars were characterized for different techniques. X-ray diffraction (XRD) was performed in a Shimadzu equipment model XRD-7000, with Cu Kα radiation, using the powder method (Osaka, Japan). Thermogravimetric analysis (TG) was done in a Shimadzu DTG-60 H (Osaka, Japan) with a nitrogen or air atmosphere of 50 mL·min^{-1} up to 700 °C and 900 °C (heating rate of 10 °C·min^{-1}). The Raman spectra were obtained in a Bruker equipment, model Senterra (Germany) equipped with a CCD detector, with an optical microscopy (OLYMPUS BX51). The spectra were done using the 633 nm laser, 2 mW,10 s and 10 co-additions. SEM images were collected in a Quanta FEG 3D (FEI/Thermo Fischer Scientific, Eindhoven, Netherlands) coupled with EDS spectrometer. Thermogravimetric analysis coupled mass spectrometer (TG-MS) were performed in a NETZSCH TGA model STA 449 F3 (Germany) coupled with NETZSCH Aëolos model QMS 403 C. For the analysis, 20 mL·min^{-1} of argon flow was used, heating rate of 10 °C·min^{-1} and final temperature of 900 °C. For FT-IR, the samples were prepared in KBr tablets and analyzed in a Perkin Elmer FTIR GX (USA) in a spectral range from 400 to 4000 cm^{-1}. Curves of potential titration were obtained at 25 °C, inert atmosphere, in a SI Analytics model Tritoline 7000 with Ag/AgCl electrode. The sample was dispersed in 20 mL solution of HCl (0.0014 mol·L^{-1}) and NaCl (0.1 mol·L^{-1}) and titrated with NaOH (0.0105 mol·L^{-1}). The samples were also characterized by N_2 adsorption/desorption using a Quantachrome Autosorb 1 (Florida, USA) after 9 h degassing at 250 °C. Elemental analysis (CHN) was performed in a CHN Perkin Elmer 2400 (CHN-PE-2400, USA).

Adsorption experiments

Different parameters were available during the adsorption experiments: adsorbent concentrations; the influence of the pH; isotherm experiments and kinetics experiments.

The Pb solutions were prepared from $(PbNO_3)_2$ (Sigma Aldrich). In order to avoid precipitation, the solution pH was set to 5 using HCl 0.1 mol.L^{-1}. The adsorption experiments were carried out using 20 mL of Pb^{2+} solution with initial concentration of 40 mg.L^{-1} and 10 mg of the adsorbent. The mixture of adsorbent and Pb solution was stirred for 2 h (OVAN shaker) and then filtered (Millipore 0.5 μm). Then, the solution was analyzed by flame atomic absorption (Agilent model AA 240 FS).

For the optimization of adsorbent concentration, 5, 10 and 20 mg of BC04 were added in 20 mL of Pb^{2+} solution with initial concentration of 40 mg.L^{-1}. The mixture of adsorbent and Pb solution was stirred for 2 h (OVAN shaker) and then filtered (Millipore 0.5 μm). Then, the solution was analyzed by flame atomic absorption (Agilent model AA 240 FS).

In 40 ppm Pb^{2+} solutions, the pH was set to 2.0, 3.0, 4.0, 5.0, 6.0, 7.0 and 8.0 (KASVI Phmeter). Then it was added 10 mg of BC04 in 20 mL of each the prepared solutions. The mixture of adsorbent and Pb solution was stirred for 2 h (OVAN shaker) and then filtered (Millipore 0.5 μm). Then, the solution was analyzed by flame atomic absorption (Agilent model AA 240 FS).

Isotherm experiments

The isotherm was performed, at room temperature, using 0.5 g·L^{-1} of adsorbent. It was prepared different solution in a [Pb^{2+}] i.e.: 0, 10, 20, 40, 60, 80 and 100 mg·L^{-1}. The mixture of adsorbent and Pb solution was stirred for 2 h (OVAN shaker) and then filtered (Millipore 0.5 μm). Then, the solution was analyzed by flame atomic absorption (Agilent model AA 240 FS).

To describe the interaction between adsorbate and adsorbent, two isotherm models were investigated. The isotherm linear fitting were performed using the models of Langmuir (Eq. 1) and Freundlich (Eq. 2): [39].

$$\frac{C_e}{q_e} = \frac{C_e}{q_m} + \frac{1}{K_L q_m} \tag{1}$$

$$\ln \quad q_e = \ln \quad K_F + \frac{1}{n} \ln C_e \tag{2}$$

where C_e is [Pb^{2+}] at equilibrium, q_e (mg·g^{-1}) is the adsorbed amount, q_m is the maximum adsorption capacity (mg·g^{-1}); K_L is Langmuir constant; K_F and n_F are Freundlich constants.

Kinetics experiments

Pb^{2+} solution of 40 mg·L^{-1} and pH 5 was used for kinetic experiments. The adsorption was measured at different times (5, 10, 15, 20,

25, 30, 40, 50, 60, 90, 120, 150 and 180 min) after adding 0.5 g·L^{-1} of adsorbent. The mixture of adsorbent and Pb solution was stirred for 2 h (OVAN shaker) and then filtered (Millipore 0.5 μm). Then, the solution was analyzed by flame atomic absorption (Agilent model AA 240 FS).

The experimental results were fitted using pseudo-first-order and pseudo-second-order models in its non-linear form, and the correlative parameters were obtained using the corresponding dynamic model formulas (Eqs. 3 and 4) (Yang et al., 2016):

$$q_t = q_e(1 - e^{-K_1 t}) \quad (3)$$

$$q_t = \frac{q_e^2 K_2 t}{1 + q_e K_2 t} \quad (4)$$

where k_1 (min^{-1}) is the pseudo-first order rate constant, k_2 (g·mg^{-1}·min^{-1}) is the pseudo-second order rate constant, q_e (mg·g^{-1}) is the Pb(II) adsorption amount at equilibrium, and q_t (mg·g^{-1}) means the Pb(II) adsorption amount at a time *t*.

Results and discussion

Characterization

In this work, we have prepared three carbon materials, ca. BC01, BC02 and BC04, heating the precursor (macauba's endocarp - MEP) with concentrated H_2SO_4 at 100 °C for 1, 2 and 4 h. This treatment is responsible for carbonization and sulfonation processes (Fig. S1). [40].

In order to assess the changes in carbon structures caused by the carbonization process, the obtained materials, BC01, BC02 and BC04, were characterized by Raman spectroscopy (Fig. 1). The presence of the two characteristic bands of carbonaceous materials, D and G bands, after the reaction confirms the occurrence of carbonization process. The D band around 1330 cm^{-1} is related to the presence of defects in organized carbon structures [41]. The G band, founded around 1570 cm^{-1}, is typical of organized graphical structures and indicates the presence of materials that have bonds between carbon atoms with sp^2 hybridization [42]. The exothermicity of sulfuric acid may have contributed to the elevation of the reaction temperature, generating hot spots that favor the pyrolysis process [40].

The crystalline structure was investigated by XRD analysis (Fig. 2) which showed a broadened peak centered in 2θ at 23° due to an amorphous carbonaceous structure [43,44]. The most pronounced peaks that appear in the diffractogram are related to silica (SiO_2, JCPDS 46–1045), an impurity present in both precursor and synthesized materials [45].

The thermal stability of the materials was evaluated by thermogravimetric analysis. The TG/DTG curves in N_2 atmosphere for the

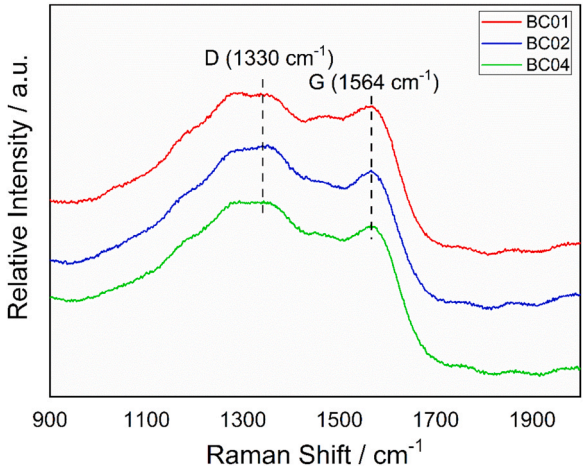

Fig. 1. Raman spectra of BC01, BC02 and BC04 highlighting the D and G bands.

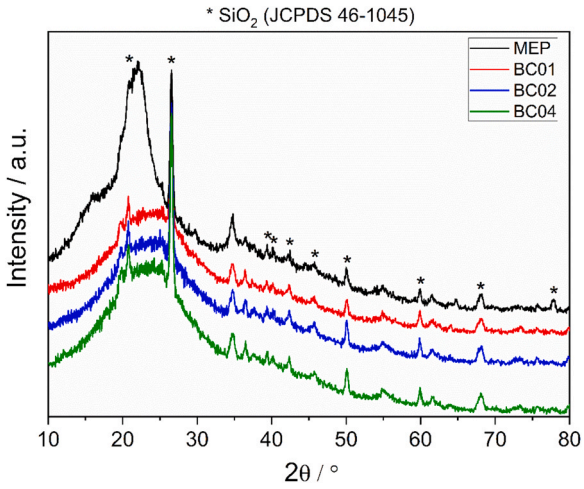

Fig. 2. X-ray diffractograms for MEP, BC01, BC02 and BC04.

precursor, MEP (Fig. 3(a)), showed a weight loss of approximately 10% up to 100 °C, due to the loss of water and small volatile molecules. The second and third loss event, centered at 294 and 351 °C, can be attributed to the thermal degradation of cellulose and hemicellulose, producing CO_2, H_2O and other small volatile molecules. At higher temperatures, the weight loss is related to the degradation of lignin, which has greater thermal stability [38].

The weight losses above 100 °C observed for the biochar materials (BC01, BC02 and BC04) may be associated with the degradation of organic matter, which was not fully carbonized during the synthesis of the material, and the degradation of the functional groups on the surface of the BC.

Comparing the TG/DTG curves obtained in an oxidizing atmosphere (Fig. 3(b)) with the curves obtained in an inert atmosphere, we observed a higher weight loss. In the DTG curves it is possible to observe a significant loss at 460 °C, especially for the carbon materials, which did not occur in an inert atmosphere. This weight loss can be attributed to the oxidation of carbonaceous materials to CO_2, according to Eq. 5: [46].

$$C_{(s)} + O_{2(g)} \rightarrow CO_{2(g)} \quad (5)$$

Considering that any further weight loss occurring in an oxidizing atmosphere is related to the oxidation of a more stable type of carbon, it is possible to estimate the approximate carbonization content for each material, c.a. 38, 30, 29% for BC04, BC02 and BC01, respectively. The percentage of residual mass in an oxidizing atmosphere can be attributed to the presence of some inorganic compound, such as silica. The results obtained confirmed the greater effectiveness of carbonization over 4 h.

The volatiles released by heating the sample in an inert atmosphere were analyzed by TG-MS for MEP and BC04 monitoring the *m/z* signal 18, 44 and 64. The TG-MS profiles (Fig. 3(c)) confirmed that the weight loss around 100 °C is related to water adsorbed on the materials. We also observed that the weight loss between 250 and 400 °C is due to water, but now associated with cellulose decomposition. The intensity of this signal was significantly reduced for BC04 sample, which can be explained by the dehydration of the precursor by sulfuric acid. The intensity of *m/z* signal 44, related to the loss of CO_2 between 200 and 400 °C, was also considerably reduced after the sulfonation, which may have been caused by reactions of deoxygenation of the cellulose by sulfuric acid, forming more stable carbonaceous structures [40]. The weight loss at around 450 °C for BC04 confirmed the previous association to the loss of CO_2.

We also observed an intense *m/z* signal 64 between 200 and 400 °C for BC04 that can be associated to SO_2 loss through the decomposition of $–SO_3H$ superficial groups.

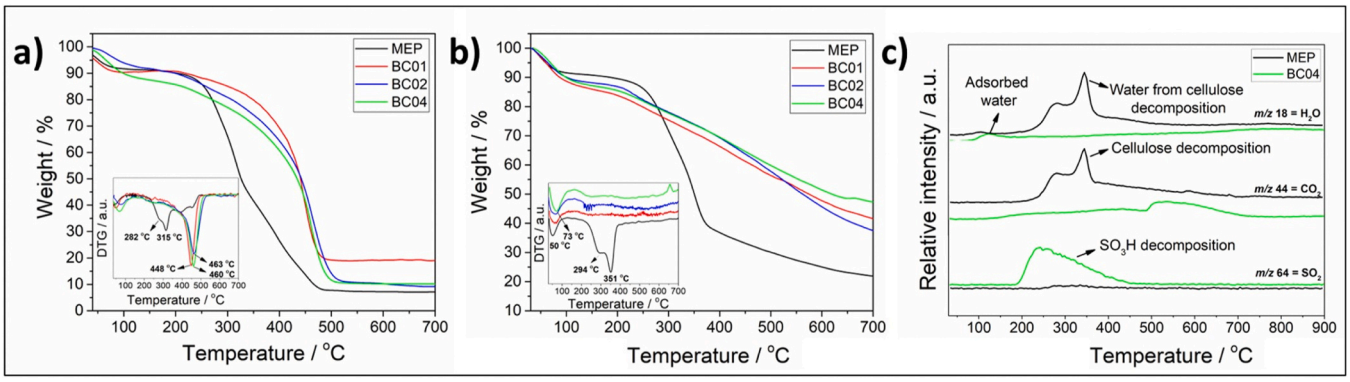

Fig. 3. (a) TG and DTG curves, in N_2 atmosphere, for MEP, BC01, BC02 and BC04; (b) TG and DTG curves, in air atmosphere, for MEP, BC01, BC02 and BC04; (c) *m/z* 18, 44 and 64 signals for MEP and BC04 during TG analysis.

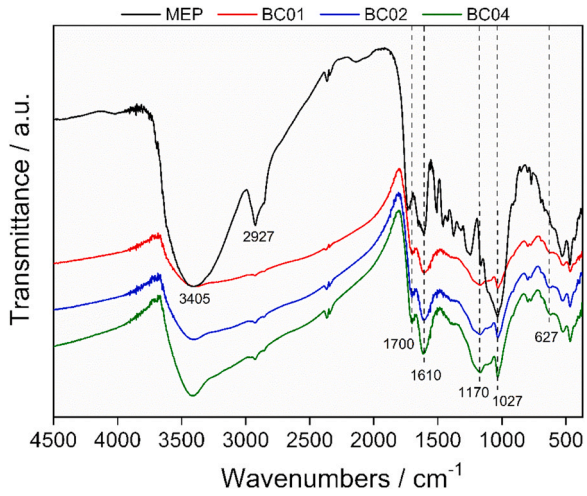

Fig. 4. FTIR spectra of the precursor MEP and the obtained materials BC01, BC02 and BC04.

The functional groups present in the materials, especially the changes after sulfonation, was identified by FTIR (Fig. 4). We identified, for MEP, characteristic bands of lignocellulosic materials. The broad and intense band around 3405 cm^{-1} is attributed to stretching of the hydroxyl group (-OH). Bands around 2927 and 1610 cm^{-1} are characteristic of aliphatic C-H stretching mode and aromatic C=C stretching vibration, respectively. The stretching modes of C=O were observed around 1700 cm^{-1} [40,47].

After carbonization and sulfonation process, significant changes were observed in the spectra. The first change was the decrease of absorptions intensities at 3405 and 2927 cm^{-1}, probably due to dehydration caused by sulfuric acid. Another change was the appearance of symmetric (1027 cm^{-1}) and asymmetric (1170 cm^{-1}) stretching of O=S=O belonging to $-SO_3$ groups and a low intensity band around 627 cm^{-1}, related to the bending vibration of -OH groups bonded to $-SO_3H$. These last changes confirmed the sulfonation for BC01, BC02 and BC04.

Fig. 5 show the scanning electron microscopy images obtained for the materials MEP, BC01, BC02 and BC04, respectively, with different magnifications. For all materials, after carbonization, is possible to observe irregular surfaces, with a heterogeneous aspect for all materials.

The qualitative analysis of the elements present in the samples was performed by EDS (Fig. S2). The platinum peak observed in all spectra comes from the metallization of the materials. In the carbon materials spectra it was possible to observe the presence of sulfur, confirming the sulfonation of the materials after reaction with sulfuric acid. Both the spectrum of the precursor and the biochars, the presence of silicon can be observed, thus proving the presence of silica in the materials,

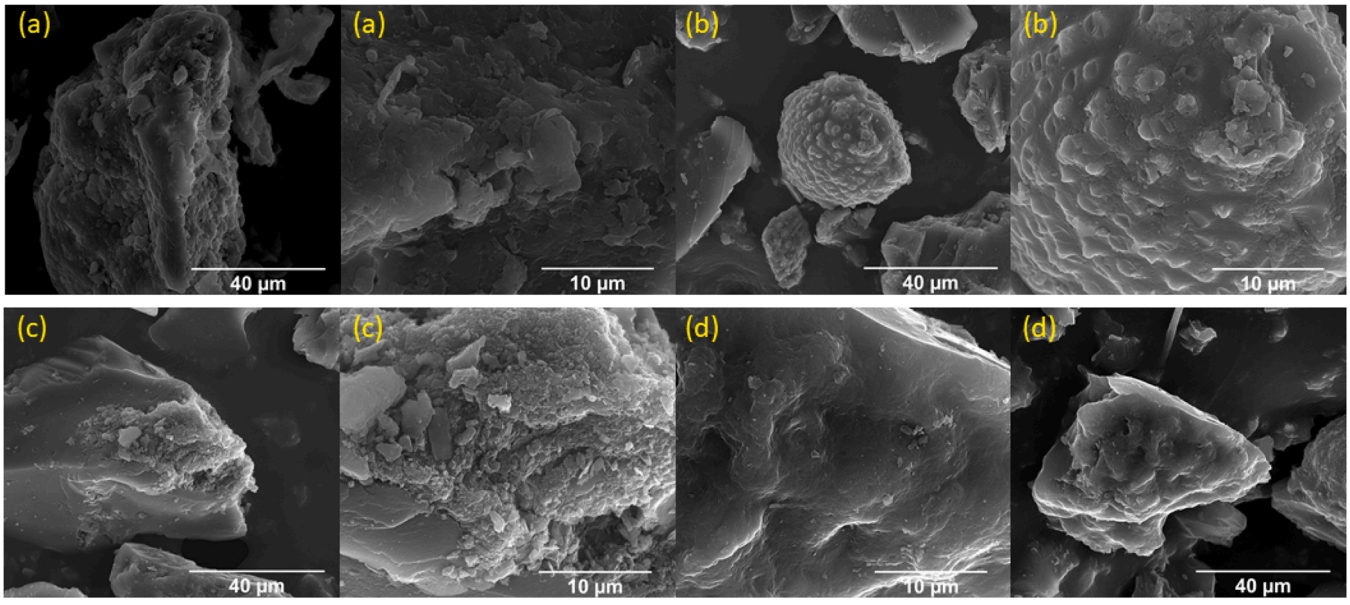

Fig. 5. Scanning electron microscopy images of (a) MEP, (b) BC01, (c) BC02 and (d) BC04.

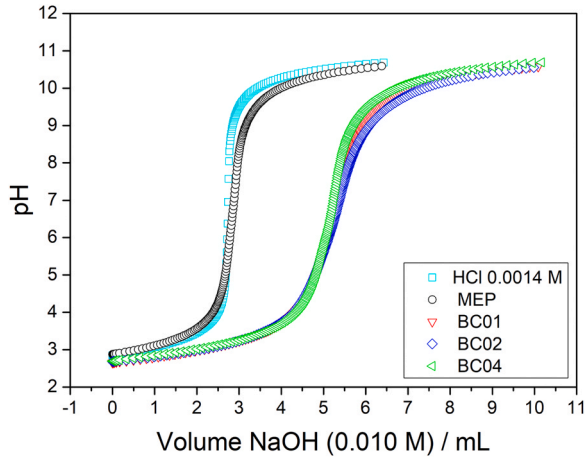

Fig. 6. Potentiometric titration curves of the materials MEP, BC01, BC02 and BC04 compared to the HCl 0.0014 M.

confirming the results obtained by XRD.

The concentration and types of acid functional groups present in the materials was determined by potentiometric titration measurements (Fig. 6).

The volume spent in the titulation of HCl solution was 2.74 mL, while for BC materials the volume was greater than 4 mL, indicating that the biochars have a high concentration of strong acid groups. This can be explained by the presence of sulfuric and sulfonic acid adsorbed on their surface.

The concentrations of the acid functional groups as a function of pKa, obtained by adjusting the potentiometric titration curves, according to the equation described by Alves et al., are shown in Table 1. [48].

The treatment of MEP with sulfuric acid provided an increase in the concentration of acid groups. The BC02 material showed a higher concentration of acid groups than the other materials. However, the BC04 material showed a higher concentration of functional groups with pKa less than 5, a range attributed to carboxylic acids, which when deprotonated, contribute to the increase of negative charge density on the adsorbent surface, favoring electrostatic interaction with Pb^{2+} ions [49].

Functional groups with pka between 5.5 and 8 are characteristic of lactones and pKa values greater than 8 attributed to phenolic groups [48]. The sulfonic groups (pKa between 1 and 2.5) were not detected in the potentiometric titration, but were identified in other characterization techniques, such as FTIR and EDS. As it is a relatively strong acid, it is believed that it contributed to the elevation of the concentration of strong acid groups on the surface of the biochars. Similar results are reported in the literature [49].

The N_2 sorption analysis is an important tool for understanding adsorption processes. The measure did not indicated a significant superficial area for BC04 ($2\ m^2 \cdot g^{-1}$). The low surface area can be justified by the fact that the material has been carbonized at low temperatures and not subjected to an activation process. Similar results are reported in the literature [40,47].

Table 2
The content of carbon, hydrogen and nitrogen on MEP, BC01, BC02 and BC04.

Sample	%C	%H	%N
MEP	44.57	5.38	0.65
BC01	46.58	3.03	0.44
BC02	53.21	3.84	0.46
BC04	47.34	3.19	0.43

The content of carbon, hydrogen and nitrogen in each material was found by elemental analysis and the results are shown in Table 2.

The carbon content did not vary significantly when comparing the precursor with materials after carbonization. The hydrogen content of the materials was reduced after carbonization, indicating that organic matter was dehydrated by the process of synthesis.

The carbon content obtained by elemental analysis differed from those calculated in the thermal analysis, since the first quantifies all types of carbon, while the latter it was considered only carbon with stable structures that is oxidized to CO_2 at higher temperatures.

Adsorption experiments

The materials produced in this work were used as adsorbents of lead ions in aqueous media. In terms of comparison, adsorption tests were also carried out with the precursor, MEP. The percentage removal of Pb^{2+} as a function of the material used is shown in Fig. 7(a).

Interestingly, treatment with sulfuric acid provided a significant increase in the effectiveness of the material for Pb^{2+} removal. Similar results were obtained for BC01, BC02 and BC04, although for BC04 the removal was slightly higher (86.0 ± 2.1%). Based on the adsorption and characterizations results, BC04 was selected for further studies.

Despite presenting a low surface area, the BC04 material removed a high amount Pb^{2+}, and it can be inferred that the adsorption process is taking place due to the interactions of this metallic ion with the functional groups present on the surface of the biochar. A mechanism that can be proposed for Pb^{2+} adsorption is ion exchange, represented in Fig. 8, since the groups $–SO_3H$ and –COOH are ionized in aqueous medium, thus electrostatically attracting the Pb^{2+} ions. [34] In addition, the presence of other functional groups on the surface of the material can also influence the adsorption process.

The adsorbent dosage was varied from 0.25 to 1 $g \cdot L^{-1}$ keeping all other variables constant. As depicted in Fig. 7(b), the greater the adsorbent concentration the greater the removal of lead ions from the solution. The removal percentage increased from 65.1% to 96.2%, which can be explained by the increase of adsorption sites, [35] and agrees with the ion exchange mechanism.

Using an adsorbent concentration of 0.5 $g \cdot L^{-1}$, it was possible to remove 85.1% of the lead(II) present in the Pb^{2+} 40 ppm solution. This concentration of adsorbent was chosen to carry out the other tests.

The pH is one of the factors that most influences the adsorption process, since the metal species present in the solution and the charges of the adsorbent active sites are dependent on it. The study of adsorption as a function of pH was carried out in the pH range between 2.0 and 8.0. In pH 6.0 and above, the Pb^{2+} ions are hydrolyzed to form the $[Pb(OH)]^+$ cation and then precipitation begins to occur in the form of

Table 1
Concentration of the acid functional groups as a function of pKa for MEP and BC materials.

Sample	Acid functional groups / $mmol \cdot g^{-1}$				
	3.5 < pKa < 5	5 < pKa < 6.0	6.5 < pKa < 8.0	8.0 < pKa < 10	Total
MEP	0.0238	0.0826	0.0825	0.180	0.369
BC01	0.250	0.225	0.127	0.458	1.06
BC02	0.281	0.229	0.186	0.522	1.22
BC04	0.371	0.160	0.113	0.282	0.926

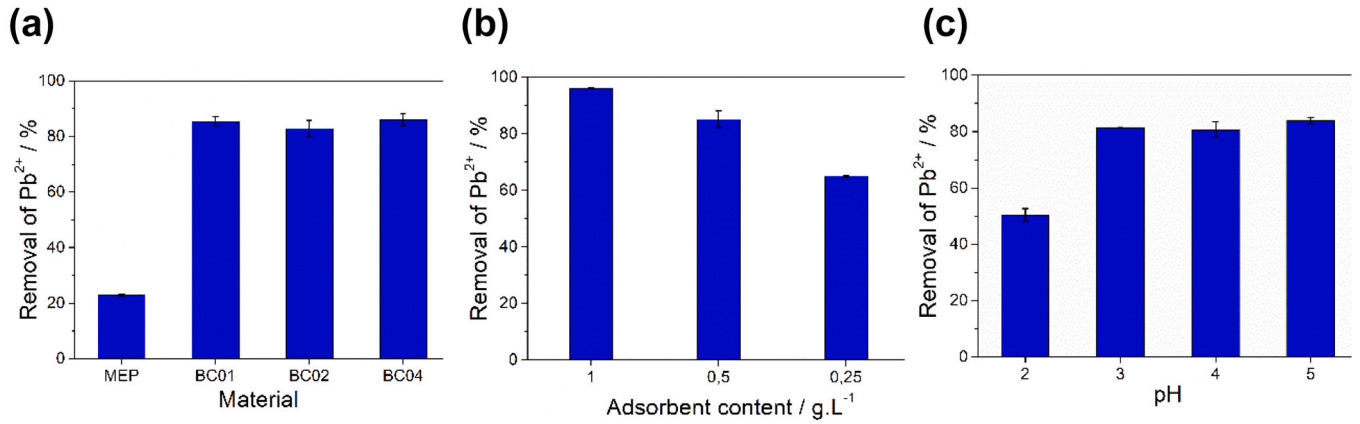

Fig. 7. (a) Removal of Pb^{2+} by MEP, BC01, BC02 and BC04; (b) Removal of Pb^{2+} as a function of adsorbent content; (c) Removal of Pb^{2+} using pH 2, 3, 4 and 5.

metal hydroxides, [35,36] turning impossible to analyze the adsorption in these pH values.

It can be seen that the lowest removal of metal ions occurred when the pH was equal to 2.0 (50.4%), which can be explained by the competition of H_3O^+ ions for the adsorbent sites (Fig. 7(c)). Another factor that may have contributed to a lesser removal is that in this pH value the groups –COOH are in a protonated form, therefore not being available for sorption. By increasing the pH, this competition is reduced and the carboxylic groups are deprotonated, causing an increase in adsorption [49–51].

The removal of lead(II) from the solution did not vary significantly for pH values between 3.0 and 5.0. At pH 5.0, removal was slightly higher (83.8%), so subsequent tests were performed at this pH value.

The pH values of the solutions after the adsorption process were lower than the initial pH values, corroborating the hypothesis that the mechanism involved in the adsorption is that of ion exchange.

Similar results are observed in the literature in which hybrid/functionalized materials were used to removal of dyes and heavy metals from wastewater. According to the authors the pH strongly influences in the adsorption process, due the interaction between deprotonated functional groups and metallic ions [52–56].

An important parameter that can be studied for different adsorbents is their selectivity for the adsorption of a specific metal ion in the presence of effluents containing mixtures of compounds. Literature studies showed that the pH directly influences the selectivity in the adsorption of heavy metals. Awual and collaborators produced hybrid materials containing surface groups for the selective adsorption of copper, cadmium and lutetium in an aqueous medium. The authors obtained excellent selectivities at specific pH values for each metallic ion [53–55].

Adsorption isotherm

The adsorption as a function of the initial concentration of lead ions was analyzed in the concentration range of 10–100 $mg{\cdot}L^{-1}$. The removal was 97.5% for the most concentrated solution and 55.0% for the lowest concentration. Fig. 9 shows the amount of lead ions adsorbed as a function of the equilibrium concentration.

It can be observed that until the concentration of 80 ppm, the increase in the initial concentration of lead provided an increase in the adsorption capacity, which can be explained by the greater availability of lead ions in solution, thus contributing for the adsorption to occur more quickly. For the concentration of 100 ppm, the same was not observed, which may have occurred due to the saturation of the adsorbent [57].

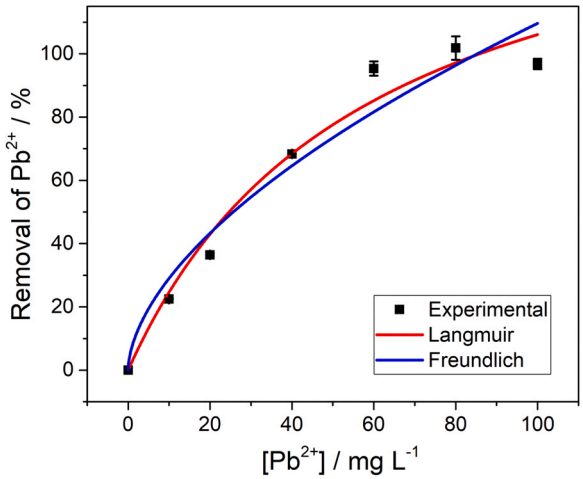

Fig. 9. Adsorption isotherm curve of lead onto BC04.

Table 3
Isotherm model parameters for adsorption of Pb(II) onto BC04.

Langmuir			Freundlich		
q_m / $mg{\cdot}g^{-1}$	K_L / $L{\cdot}mg^{-1}$	R^2	n_F	K_F / $mg{\cdot}g^{-1}$	R^2
109.9	0.3745	0.9919	3.001	33.75	0.9616

The Langmuir and Freundlich constants obtained from the isotherms and the correlation coefficients are shown in Table 3.

The experimental data were better adjusted to the Langmuir model, as can be seen by the correlation values (R^2), so the adsorption is limited to the monolayer. Moreover, the Langmuir model consider that adsorption sites are all energetically equivalent (homogeneous), [58] corroborating again with the ion exchange mechanism. The maximum adsorption capacity was 104.2 $mg{\cdot}g^{-1}$, a result comparable with other materials reported in the literature (Table 4).

The most common materials used to the lead adsorption are activated carbons, with a high superficial area, as demonstrated in Table 4. Compared to the literature, the adsorption results from this work is promising, since the BC materials have a similar efficiency. Moreover,

Fig. 8. Schematic figure showing the adsorption mechanism by ionic exchange.

Table 4
Capacity adsorption (q_{MAX}) for coals produced from different precursors in the literature.

Precursor	q_{MAX} / mg.g^{-1}	S_{BET} / m^2.g^{-1}	Reference
Wood waste	149.2	1196	Teong et. al., 2021 [59]
Rice Rusk	492	2786	Zhang et. al., 2020 [60]
Pistachio wood	190.2	1884	Sajjadi et. Al., 2019 [61]
Sludge	27.7	86	Li et. al., 2019 [62]
Cigarretes Wastes	71.4	47	Manfrin et. al., 2021 [63]
Mangosteen peel	130.5	424	Kongsune et. al., 2021 [64]
Sugar cane bagasse	135.5	69	Tao et al., 2015 [65]
Cotton stalks	119.9	1570	Li et al., 2010 [66]
Almond shell	112.0	1074	Largitte et al., 2016 [57]
Dindé stone	50.0	1029	Largitte et al., 2016 [57]
Guava seed	96.0	1201	Largitte et al., 2016 [57]
Coffee waste	63.3	890	Boudrahem et al., 2009 [51]
Macauba's endocarp	337,74	423	Rios et al., 2023 [67]
Macauba's endocarp	104.2	2	This work

1 mol – 207,2 g
0,00163 mol – x
X = 0,3377 g = 337,74

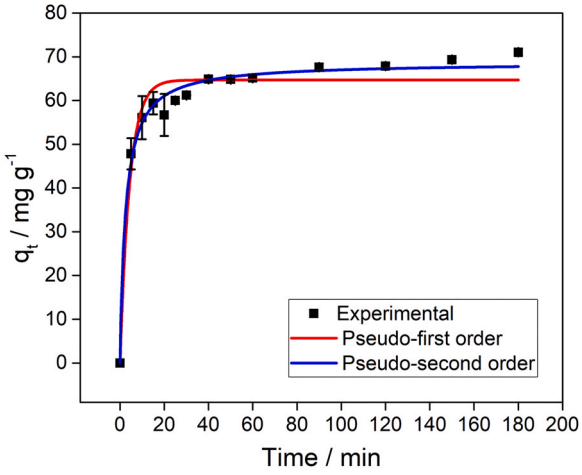

Fig. 10. Adsorption kinetics of lead onto BC04.

they have low superficial area and are produced from a residual biomass using a low temperature sulfonated process (100 °C), while the other materials need two or more steps using high temperatures (400–900 °C) for carbonization and physico or chemical activation.

The regeneration study in adsorption process is an important parameter to evaluated the cost-effectiveness of the material. Despite that, the production process of the materials proposed in this work is cheaper than most of the carbon materials proposed in the literature for this purpose, since most of them produce activated carbons with high temperatures for both carbonization and activation process.

Adsorption kinetics

Fig. 10 shows the kinetics curve for the removal of lead ions by material BC04. It can be observed that the initial sorption is very fast. In the first 5 min approximately 62.7% of the lead present in the solution was removed and in approximately 40 min the system already reaches adsorption equilibrium. This can be justified by the greater availability of adsorption sites in the beginning of the process. As the concentration of Pb2 + increases in the functional groups on the surface of the adsorbent, the accessibility to the sorption sites is hampered, which decreases the rate of adsorption. Also, there may also be repulsion between the ions present on the surface of the adsorbent and the ions present in the solution, causing the process to slow down [51,57].

In 40 min, a removal of 85.1% was observed, similar to that obtained for the other tests that were carried out in 120 min. After that time, there were no significant variations in removal with 93.1% of removal in the final time.

The adsorption process was also described using two kinetic models in its non-linear form, pseudo-first order and pseudo-second order (Fig. 10 and Table 5). The higher R^2 value for the pseudo-second-order kinetic model indicated the lead sorption process on BC04 may be ruled by chemical forces, reinforcing the possibility of ion exchange mechanism. Also, this result agreed with several studies that have found pseudo-second order model was the best fit for lead adsorption onto activated carbons and biochars with high adsorption kinetics [63,68–70].

Conclusion

This work demonstrated that it is possible to carbonize and functionalize a residual biomass, macauba's endocarp, with sulfuric acid at low temperatures and times, in order to produce a new adsorbent material for lead(II) adsorption. Characterizations by XRD, Raman and TG confirmed the carbonization and FTIR and TG-MS also confirmed the presence of -SO_3H groups.

Adsorption studies have shown that BC01, BC02 and BC04 materials have similar capacities adsorption of lead(II), adsorption increases as the amount of adsorbent increases, ca. 65.1–96.2%, indicating that the amount of active adsorption sites is crucial for the adsorption. Also, it was found that the best pH for the process is 5.

Langmuir isotherm model presented the best fit to the adsorption data, indicating homogeneous sites of adsorption. Kinetic experiments revealed an initial rapid adsorption of lead metal ions and the data were better fitted by pseudo-second order model.

Table 5
Kinetic model parameters for adsorption of Pb(II) onto BC04.

	Pseudo-first order			Pseudo-second order		
	q_e / mg·g^{-1}	K_1 / min^{-1}	R^2	q_e / mg·g^{-1}	K_2 / g·mg^{-1}·min^{-1}	R^2
BC04	64.7	0.230	0.949	68.7	0.00579	0.987

The adsorption studies and the characterization by potentiometric titration are suggesting that the lead adsorption onto the biochar produced in this work is mainly ruled by chemical affinity between metal ions and adsorbent surfaces rich in –COO- and –SO3- groups. The presence of different acidic groups, and especially those with pka < 5 attributed to carboxylic acids, seem to be involved in the adsorption, since they can be deprotonated, increasing the density of negative charge on the surface, leading to a increasing of lead ions adsorption.

Declaration of Competing Interest

The authors declare that they have no known competing financial interests or personal relationships that could have appeared to influence the work reported in this paper.

Acknowledgments

This work was supported by the CNPq, CAPES, FAPEMIG and INCT Midas. The authors thank the Microscopy Center UFMG for SEM images.

Appendix A. Supporting information

Supplementary data associated with this article can be found in the online version at doi:10.1016/j.nxmate.2023.100028.

References

[1] E. Abu-Danso, S. Peräniemi, T. Leiviskä, A. Bhatnagar, Environ. Pollut. 242 (2018) 1988–1997.
[2] F. Fu, Q. Wang, J. Environ. Manag. 92 (2011) 407–418.
[3] A.E. Burakov, E.V. Galunin, I.V. Burakova, A.E. Kucherova, S., A.G. Tkachev, V.K. Gupta, Environ. Saf. 148 (2018) 702–712.
[4] R. Barbosa, N. Lapa, H. Lopes, A. Günther, D. Dias, B. Mendes, J. Colloid Interface Sci. 424 (2014) 27–36.
[5] Y. Ren, N. Li, J. Feng, T. Luan, Q. Wen, Z. Li, M. Zhang, J. Colloid Interface Sci. 367 (2012) 415–421.
[6] C.B. Godiya, X. Cheng, D. Li, Z. Chen, X. Lu, J. Hazard. Mater. 364 (2019) 28–38.
[7] M.S. Salman, H. Znad, M.N. Hasan, M.M. Hasan, Microchem. J. 160 (2021) 105765.
[8] W.S. Wan Ngah, L.C. Teong, M.A.K.M. Hanafiah, Carbohydr. Polym. 83 (2011) 1446–1456.
[9] Q. Chen, Y. Yao, X. Li, J. Lu, J. Zhou, Z. Huang, J. Water Process Eng. 26 (2018) 289–300.
[10] R. Choumane, S. Peulon, Chem. Eng. J. 423 (2021) 130161.
[11] W. Peng, G. Han, Y. Cao, K. Sun, S. Song, Colloids Surf. A: Physicochem. Eng. Asp. 556 (2018) 266–272.
[12] S. Amiri, A. Asghari, V. Vatanpour, M. Rajabi, J. Environ. Manag. 294 (2021) 112918.
[13] J. Qu, Q. Meng, X. Lin, W. Han, Q. Jiang, L. Wang, Q. Hu, L. Zhang, Y. Zhang, Sci. Total Environ. 752 (2021) 141854.
[14] X. Luo, M. Shen, Z. Huang, Z. Chen, Z. Chen, B. Lin, L. Cui, Environ. Res. 190 (2020) 110014.
[15] Md.R. Awual, Mater. Sci. Eng.: C. 101 (2019) 686–695.
[16] Md.R. Awual, Md.M. Hasan, J. Mol. Liq. 294 (2019) 111679.
[17] Md.R. Awual, J. Mol. Liq. 284 (2019) 502–510.
[18] Md.S. Salman, H. Znad, Md.N. Hasan, Md.M. Hasan, Microchem. J. 160 (2021) 105765.
[19] Md Awual, J. Environ. Chem. Eng. 7 (2019) 103124.
[20] Md.R. Awual, J. Clean. Prod. 228 (2019) 1311–1319.
[21] Md.R. Awual, J. Environ. Chem. Eng. 7 (2019) 103087.
[22] A. Shahat, Md.R. Awual, Md.A. Khaleque, Md.Z. Alam, M. Naushad, A.M.S. Chowdhury, Chem. Eng. J. 273 (2015) 286–295.
[23] Md.R. Awual, Chem. Eng. J. 266 (2015) 368–375.
[24] Md.R. Awual, A. Islam, Md.M. Hasan, M.M. Rahman, A.M. Asiri, Md.A. Khaleque, Md.C. Sheikh, J. Clean. Prod. 224 (2019) 920–929.
[25] Md.R. Awual, Md.M. Hasan, J. Iqbal, A. Islam, Md.A. Islam, A.M. Asiri, M.M. Rahman, Microchem. J. 154 (2020) 104585.
[26] Y. Wang, H. Li, S. Lin, Water 14 (2022) 1–11.
[27] J. Wu, T. Wang, J. Wang, Y. Zhang, W.-P. Pan, Sci. Total Environ. 754 (2021) 142150.
[28] W. Yu, J. Hu, Y. Yu, D. Ma, W. Gong, H. Qiu, Z. Hu, and H.-w, Gao, *Sci. Total Environ.* 750 (2021) 141545.
[29] T. Zhao, Y. Yao, D. Li, F. Wu, C. Zhang, B. Gao, Sci. Total Environ. 640–641 (2018) 73–79.
[30] N. Chaukura, W. Gwenzi, N. Mupatsi, D.T. Ruziwa, C. Chimuka, Water, Air, Soil Pollut. 228 (2016) 7.
[31] W.-H. Huang, D.-J. Lee, C. Huang, Bioresour. Technol. 319 (2021) 124100.
[32] E.C. Nnadozie, P.A. Ajibade, Microporous Mesoporous Mater. 309 (2020) 110573.
[33] G.-X. Yang, H. Jiang, Water Res. 48 (2014) 396–405.
[34] M. Ahmad, A.U. Rajapaksha, J.E. Lim, M. Zhang, N. Bolan, D. Mohan, M. Vithanage, S.S. Lee, Y.S. Ok, Chemosphere 99 (2014) 19–33.
[35] H. Yang, S. Ye, Z. Zeng, G. Zeng, X. Tan, R. Xiao, J. Wang, B. Song, L. Du, M. Qin, Y. Yang, F. Xu, Chem. Eng. J. 397 (2020) 125502.
[36] G.K. Souza, F.B. Scheufele, T.L.B. Pasa, P.A. Arroyo, N.C. Pereira, Fuel 165 (2016) 360–366.
[37] E.C.G. Aguieiras, E.D. Cavalcanti-Oliveira, A.M. de Castro, M.A.P. Langone, D.M.G. Freire, Fuel 135 (2014) 315–321.
[38] S.S. Vieira, Z.M. Magriotis, N.A.V. Santos, M. d G. Cardoso, A.A. Saczk, Chem. Eng. J. 183 (2012) 152–161.
[39] M. Ghasemi, M. Naushad, N. Ghasemi, Y. Khosravi-fard, J. Ind. Eng. Chem. 20 (2014) 2193–2199.
[40] E.M. Santos, A.P. d C. Teixeira, F.G. da Silva, T.E. Cibaka, M.H. Araújo, W.X.C. Oliveira, F. Medeiros, A.N. Brasil, L.S. de Oliveira, R.M. Lago, Fuel 150 (2015) 408–414.
[41] Y. Wang, D.C. Alsmeyer, R.L. McCreery, Chem. Mater. 2 (1990) 557–563.
[42] R.P. Vidano, D.B. Fischbach, L.J. Willis, T.M. Loehr, Solid State Commun. 39 (1981) 341–344.
[43] R. Pereira Lopes, D. Astruc, Coord. Chem. Rev. 426 (2021) 213585.
[44] S. Neusatz Guilhen, S. Rovani, L. Pitol Filho, D. Alves Fungaro, Chem. Eng. Commun. 206 (2019) 1354–1366.
[45] H. Kobayashi, H. Matsuhashi, T. Komanoya, K. Hara, A. Fukuoka, Chem. Commun. 47 (2011) 2366–2368.
[46] P.H. Ramos, M.C. Guerreiro, E.C. Resende, M. Golçalves, Quim. Nova 32 (2009) 1139–1143.
[47] M. Mantovani, E.M. Aguiar, W.A. Carvalho, D. Mandelli, M. Golçalves, Quim. Nova 38 (2015) 526–532.
[48] L.A. Alves, A.H. de Castro, F.G. de Mendonça, J.P. de Mesquita, Appl. Surf. Sci. 370 (2016) 486–495.
[49] F.V. Hackbarth, F. Girardi, J.C. Santos, A.A.U. de Souza, R.A.R. Boaventura, S.M.A.G.U. de Souza, V.J.P. Vilar, Chem. Eng. J. 269 (2015) 359–370.
[50] T.A. Saleh, V.K. Gupta, A.A. Al-Saadi, J. Colloid Interface Sci. 396 (2013) 264–269.
[51] F. Boudrahem, F. Aissani-Benissad, H. Aït-Amar, J. Environ. Manag. 90 (2009) 3031–3039.
[52] Md.S. Salman, Md.C. Sheikh, Md.M. Hasan, Md.N. Hasan, K.T. Kubra, A.I. Rehan, Mrs E. Awual, A.I. Rasee, R.M. Waliullah, M.S. Hossain, Md.A. Khaleq, A.K.D. Alsukaibi, H.M. Alshammari, Md.R. Awual, Appl. Surf. Sci. 622 (2023) 157008.
[53] Md.S. Salman, Md.N. Hasan, Md.M. Hasan, K.T. Kubra, Md.C. Sheikh, A.I. Rehan, R.M. Waliullah, A.I. Rasee, Mrs E. Awual, M.S. Hossain, A.K.D. Alsukaibi, H.M. Alshammari, Md.R. Awual, J. Mol. Struct. 1282 (2023) 13529.
[54] Md.M. Hasan, K.T. Kubra, Md.N. Hasan, Mrs E. Awual, Md.S. Salman, Md.C. Sheikh, A.I. Rehan, A.I. Rasee, R.M. Waliullah, Md.S. Islam, S. Khandaker, A. Islam, M.S. Hossain, A.K.D. Alsukaibi, H.; M. Alshammari, Md.R. Awual, J. Mol. Liq. 371 (2023) 121125.
[55] Md.N. Hasan, Md.S. Salman, Md.M. Hasan, K.T. Kubra, Md.C. Sheikh, A.I. Rehan, A.I. Rasee, Mrs E. Awual, R.M. Waliullah, M.S. Hossain, A. Islam, S. Khandaker, A.K.D. Alsukaibi, H.M. Alshammari, Md.R. Awual, J. Mol. Struct. 1276 (2023) 134795.
[56] A. Islam, S.H. Teo, Y.H. Taufiq-Yap, C.H. Ng, D.N. Vo, M.L. Ibrahim, Md.M. Hasan, M.A.R. Khan, A.S.M. Nur, Md.R. Awual, Resour., Conserv. Recycl. 175 (2021) 105849.
[57] L. Largitte, T. Brudey, T. Tant, P.C. Dumesnil, P. Lodewyckx, Microporous Mesoporous Mater. 219 (2016) 265–275.
[58] K.C. Bedin, A.C. Martins, A.L. Cazetta, O. Pezoti, V.C. Almeida, Chem. Eng. J. 286 (2016) 476–484.
[59] C.Q. Teong, H.D. Setiabudi, N.A.S. El-Arish, M.B. Bahari, L.P. Teh, Mater. Today.: Proc. 42 (2021) 165–171.
[60] Y. Zhang, X. Song, P. Zhang, H. Gao, C. Ou, X. Kong, Chemosphere 245 (2020) 125587.
[61] S.-A. Sajjadi, A. Meknati, E.C. Lima, G.L. Dotto, D.I. Mendoza-Castillo, I. Anastopoulos, F. Alakhras, E.I. Unuabonah, P. Singh, A. Hosseini-Bandegharaei, J. Environ. Manag. 236 (2019) 34–44.
[62] L.Y. Li, X. Gong, O. Abida, Waste Manag. 87 (2019) 375–386.
[63] J. Manfrin, A.C. Gonçalves Jr, D. Schwantes, E. Conradi Jr, J. Zimmermann, G.L. Ziemer, J. Environ. Chem. Eng. 9 (2021) 104980.
[64] P. Kongsune, S. Rattanapan, R. Chanajaree, Groundw. Sustain. Dev. 12 (2021) 100524.
[65] H.-C. Tao, H.-R. Zhang, J.-B. Li, W.-Y. Ding, Bioresour. Technol. 192 (2015) 611–617.
[66] K. Li, Z. Zheng, Y. Li, J. Hazard. Mater. 181 (2010) 440–447.
[67] R.D.G. Rios, P.J.B. Bueno, J.C.S. Terra, F.C.C. Moura, Environ. Sci. Pollut. Res. 30 (2023) 31881–31894.
[68] S. Wongrod, S. Simon, G. Guibaud, P.N.L. Lens, Y. Pechaud, D. Huguenot, E.D. van Hullebusch, J. Environ. Manag. 219 (2018) 277–284.
[69] M.T. Amin, A.A. Alazba, M. Shafiq, Chem. Phys. Lett.722 (2019) 64–73.
[70] J. Zhang, J. Shao, Q. Jin, X. Zhang, H. Yang, Y. Chen, S. Zhang, H. Chen, Sci. Total Environ. 716 (2020) 137016.